The Electronic Structure of the Flavin Cofactor in DNA Photolyase

Stefan Weber,*,† Klaus Möbius,† Gerald Richter,‡ and Christopher W. M. Kay†

Contribution from the Institute of Experimental Physics, Free University Berlin, Arnimallee 14, 14195 Berlin, Germany, and Institute of Organic Chemistry and Biochemistry, Technical University Munich, Lichtenbergstrasse 4, 85747 Garching, Germany

Received September 18, 2000. Revised Manuscript Received February 13, 2001

Abstract: Density functional theory is used to calculate the electronic structure of the neutral flavin radical, $FADH^{\bullet}$, formed in the light-induced electron-transfer reaction of DNA repair in *cis,syn*-cyclobutane pyrimidine dimer photolyases. Using the hybrid B3LYP functional together with the double-ζ basis set EPR-II, ^{1}H, ^{13}C, ^{15}N, and ^{17}O isotropic and anisotropic hyperfine couplings are calculated and explained by reference to the electron densities of the highest occupied molecular orbital and of the unpaired spin distribution on the radical. Comparison of calculated and experimental hyperfine couplings obtained from EPR and ENDOR/TRIPLE resonance leads to a refined structure for the FAD cofactor in *Escherichia coli* DNA photolyase. Hydrogen bonding at N3H, O4, and N5H results in significant changes in the unpaired spin density distribution and hyperfine coupling constants. The calculated electronic structure of $FADH^{\bullet}$ provides evidence for a superexchange-mediated electron transfer between the cyclobutane pyrimidine dimer lesion and the 7,8-dimethyl isoalloxazine moiety of the flavin cofactor via the adenine moiety.

1. Introduction

DNA photolyases are flavoenzymes that catalyze the photorepair of *cis,syn*-cyclobutane thymine dimers, T⟨⟩T, formed in UV-irradiated ($\lambda \leq 300$ nm) cellular DNA from two adjacent thymine bases T.[1−8] The enzyme binds to the damaged part of the DNA strand and catalyzes its repair when exposed to near-UV or visible light ($300 < \lambda < 500$ nm). The putative reaction mechanism proposes that the flavin cofactor is initially in its fully reduced form, $FADH^{-}$.[9,10] Following light excitation, $^{*}FADH^{-}$ transfers one electron to T⟨⟩T:

$$^{*}FADH^{-} + T\langle\rangle T \underset{k_{-1}}{\overset{k_1}{\rightleftharpoons}} FADH^{\bullet} + T\langle\rangle T^{\bullet-} \qquad (1)$$

Following electron transfer, the two bonds between the thymines break:

$$T\langle\rangle T^{\bullet-} \xrightarrow{k_2} TT^{\bullet-} \qquad (2)$$

Subsequently, an electron is transferred back to the neutral flavin semiquinone radical, $FADH^{\bullet}$:

$$FADH^{\bullet} + TT^{\bullet-} \xrightarrow{k_3} FADH^{-} + TT \qquad (3)$$

Thus, the DNA lesion is repaired and the catalytic cycle is completed, with the flavin returned to its initial state. The efficiency of the overall process depends on the relative rates of dimer splitting, eq 2, and back electron transfer, the reverse of eq 1.[4] Both of these may be manipulated in order to increase the quantum yield of repair. The binding of a substrate by an enzyme typically increases the strain in the reactant, by making it resemble a transition state, which increases the driving force, ΔG, and reduces the activation energy, $\Delta G^{\ddagger}$, thus increasing the rate of dimer splitting.[4,11] Alternatively, the rate of back electron transfer, k_{-1}, may be reduced. Apart from the driving force and the reorganization energy, according to Marcus electron transfer theory,[12,13] the rate of electron transfer is dependent on the electronic coupling between the donor and acceptor. Therefore, knowledge of both the spatial and electronic structures is crucial for understanding electron-transfer kinetics. While the three-dimensional structure of the DNA photolyase enzyme from *Escherichia coli* is available at a resolution of 2.3 Å,[14] determination of the electronic structure requires high-resolution magnetic resonance studies as they—for paramagnetic intermediates—provide access to the system's wave function through an analysis of its hyperfine couplings (hfc's). The link between geometry and electron density distribution may be provided by quantum chemical computations.

To our knowledge, the first ab initio molecular orbital (MO) study of flavin radicals was made by Platenkamp and co-workers.[15] Using geometries based on crystal structures, they

* Corresponding author. Phone: +49 (30) 838-56139. Fax: +49 (30) 838-56046. E-mail: Stefan.Weber@physik.fu-berlin.de.
† Free University Berlin.
‡ Technical University Munich.

(1) Kim, S.-T.; Sancar, A. *Photochem. Photobiol.* **1993**, *57*, 895−904.
(2) Sancar, A. *Biochemistry* **1994**, *33*, 2−9.
(3) Heelis, P. F.; Hartman, R. F.; Rose, S. D. *Chem. Soc. Rev.* **1995**, *24*, 289−297.
(4) Heelis, P. F.; Hartman, R. F.; Rose, S. D. *J. Photochem. Photobiol. A Chem.* **1996**, *95*, 89−98.
(5) Sancar, A. *Science* **1996**, *272*, 48−49.
(6) Zhao, X.; Mu, D. *Histol. Histopathol.* **1998**, *13*, 1179−1182.
(7) Todo, T. *Mutat. Res.* **1999**, *434*, 89−97.
(8) Deisenhofer, J. *Mutat. Res.* **2000**, *460*, 143−149.
(9) Sancar, G. B.; Jorns, M. S.; Payne, G.; Fluke, D. J.; Rupert, C. S.; Sancar, A. *J. Biol. Chem.* **1987**, *262*, 492−498.
(10) Payne, G.; Heelis, P. F.; Rohrs, B. R.; Sancar, A. *Biochemistry* **1987**, *26*, 7121−7127.
(11) Langenbacher, T.; Zhao, X.; Bieser, G.; Heelis, P. F.; Sancar, A.; Michel-Beyerle, M. E. *J. Am. Chem. Soc.* **1997**, *119*, 10532−10536.
(12) Marcus, R. A.; Sutin, N. *Biochim. Biophys. Acta* **1985**, *811*, 265−322.
(13) Kuznetsov, A. M. *Charge Transfer in Physics, Chemistry and Biology: Physical Mechanisms of Elementary Processes and an Introduction to the Theory*; Gordon and Breach Publishers: Luxembourg, 1995.
(14) Park, H.-W.; Kim, S.-T.; Sancar, A.; Deisenhofer, J. *Science* **1995**, *268*, 1866−1872.

10.1021/ja003426m CCC: $20.00
Published on Web 03/29/2001

calculated spin densities with restricted (RHF) and unrestricted (UHF) Hartree−Fock self-consistent field methods. More recently, theoretical studies of flavins in different oxidation and protonation states have been presented by Meyer et al.[16] and Zheng and Ornstein.[17] Meyer and co-workers carried out structural optimizations in order to determine heats of formation and relative energies with both semiempirical PM3 and ab initio (restricted open-shell Hartree−Fock (ROHF) with a 6-31G* basis set) MO methods on 10-methyl isoalloxazine. For structural optimizations of the closed- and open-shell systems of 7,8,10-trimethyl isoalloxazine (lumiflavin), Zheng and Ornstein used ab initio RHF/6-31G* and UHF/6-31G*, respectively. The same group also calculated Mulliken spin densities which, however, are not easily compared with measurable quantities such as hfc's. Recently, Lee and co-workers presented a geometry optimization of the neutral flavin radical in its quartet state, i.e., ^{4}FADH•, using both UHF and ROHF methods and the B3LYP functional, all in conjunction with the 6-31G* basis set.[18] They also showed the spin density distribution of the same species, which was initially thought to play a role in the photoactivation of the catalytically inert DNA photolyase enzyme.[19−21] However, recent results from Aubert and co-workers show that this process originates from the excited doublet state rather than the quartet state of the neutral flavin radical.[22]

Today, modern density functional theory (DFT)-based approaches[23−26] permit molecular and electronic structures to be predicted for relatively large systems[27−30] where traditional wave function-based techniques, such as configuration interaction or coupled cluster methods, are unrealistic due to their high computational demands. To validate these computations, however, the spin density distribution derived from such calculations should be compared to a measurable quantity, such as the system's hfc's, which have been determined for many biologically relevant radicals including the DNA photolyase enzyme.[31] Only in this way can the quality of the parameters required for modeling electron transfer be controlled and improved.

In our previous contribution,[31] we took advantage of the fact that FADH$^-$ is reversibly oxidized to FADH• during isolation and purification of DNA photolyase.[10,32] A radical thus produced can be viewed as a naturally occurring spin-label at the active site of the enzyme. With the aid of electron paramagnetic resonance (EPR), electron−nuclear double resonance (ENDOR), and electron−nuclear−nuclear triple-resonance (TRIPLE) techniques, it was possible to determine all major proton hfc's on the 7,8-dimethyl isoalloxazine ring.[31] By TRIPLE, the relative signs of hfc's could also be determined. The hfc's provide an indirect probe of the electron density of the frontier orbital, the singly occupied MO (SOMO), as spin density at the protons usually arises from spin polarization and/or hyperconjugation with the main π-electron system situated on the heavy atoms. Here, we present hybrid DFT calculations on the FADH• cofactor in DNA photolyase from *E. coli*, with a twofold aim in mind: first, to test the quality of the X-ray structure and the DFT method, by a comparison of experimentally determined hfc's with those calculated using the X-ray structure and an "optimized" structure, and second, to observe the effect of adding a pseudo-protein environment to the flavin cofactor on those hfc's. To the best of our knowledge, this work represents the first quantum chemical study of a neutral flavin radical cofactor that takes into account the specific environment of an apoprotein in order to elucidate mechanistic aspects of its enzymatic function.

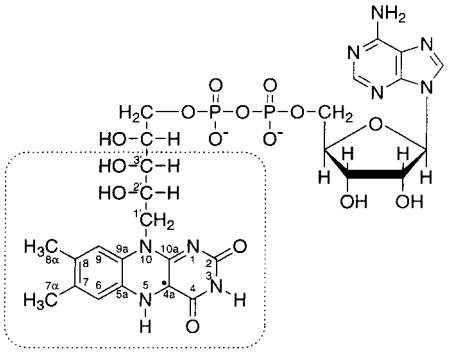

Figure 1. Molecular structure and numbering scheme of the flavin cofactor in its radical form, FADH•, in DNA photolyase. The atoms in the dotted rectangle have been considered in the DFT calculations of spin densities and hfc's (see text for details).

2. Computational Methods

The heavy-atom coordinates for FADH• used for the calculations were obtained from the crystal structure of the DNA photolyase enzyme from *E. coli*, as determined by Park et al.[14] and obtained from the Protein Data Bank (accession number 1DNP) of the Research Collaboratory for Structural Bioinformatics. The crystal structure atom coordinates correspond to the FAD in its neutral radical state, FADH•.[14] Hydrogens were added using standard bond lengths and angles. For computational purposes, the ribityl side chain attached to N10 in the 7,8-dimethyl isoalloxazine moiety of FAD was truncated at position C3′, as indicated in Figure 1. This cutoff position is well removed from the main π-electron system, and therefore, the neglect of atoms beyond this point has a negligible effect on the electron spin density distribution of the free radical.

It has been shown that the hydrogen atoms at N3 and N5 and the carbonyl oxygen O4 attached to C4 of FADH• are within hydrogen-bonding distance of the amino acids Asp-372, Asn-378, and Asp-374 in the protein backbone, respectively.[14] In our calculations of the electron spin density distribution and hfc's, we have included fragments of these amino acids that were placed at their crystallographically determined positions (see below). At a distance of 3.5 Å from N5, N10, and C4a, the side chain of Arg-344, which is positively charged at physiological pH, is also found. In order not to disregard possible effects of this cationic polar amino acid side chain on the spin density

(15) Platenkamp, R. J.; Palmer, M. H.; Visser, A. J. W. G. *J. Mol. Struct.* **1980**, *67*, 45−64.
(16) Meyer, M.; Hartwig, H.; Schomburg, D. *J. Mol. Struct. (THEOCHEM)* **1996**, *364*, 139−149.
(17) Zheng, Y.-J.; Ornstein, R. L. *J. Am. Chem. Soc.* **1996**, *118*, 9402−9408.
(18) Lee, E.; Medvedev, E. S.; Stuchebrukhov, A. A. *J. Phys. Chem. B* **2000**, *104*, 6894−6902.
(19) Heelis, P. F.; Sancar, A. *Biochemistry* **1986**, *25*, 8163−8166.
(20) Heelis, P. F.; Payne, G.; Sancar, A. *Biochemistry* **1987**, *26*, 4634−4640.
(21) Okamura, T.; Sancar, A.; Heelis, P. F.; Hirata, Y.; Mataga, N. *J. Am. Chem. Soc.* **1989**, *111*, 5967−5969.
(22) Aubert, C.; Vos, M. H.; Mathis, P.; Eker, A. P. M.; Brettel, K. *Nature* **2000**, *405*, 586−590.
(23) Hohenberg, P.; Kohn, W. *Phys. Rev.* **1964**, *136*, B864−B871.
(24) Kohn, W.; Sham, L. J. *Phys. Rev.* **1965**, *140*, A1133−A1138.
(25) Parr, R. G.; Yang, W. *Density-Functional Theory of Atoms and Molecules*; Oxford University Press: Oxford, 1989.
(26) Koch, W.; Holthausen, M. C. *A Chemist's Guide to Density Functional Theory*; Wiley-VCH: Weinheim, 2000.
(27) Himo, F.; Eriksson, L. A. *J. Phys. Chem. B* **1997**, *101*, 9811−9819.
(28) Niemz, A.; Rotello, V. M. *J. Am. Chem. Soc.* **1997**, *119*, 6833−6836.
(29) O'Malley, P. J. *J. Am. Chem. Soc.* **1999**, *121*, 3185−3192.
(30) Sinnecker, S.; Koch, W.; Lubitz, W. *Phys. Chem. Chem. Phys.* **2000**, *2*, 4772−4778.
(31) Kay, C. W. M.; Feicht, R.; Schulz, K.; Sadewater, P.; Sancar, A.; Bacher, A.; Möbius, K.; Richter, G.; Weber, S. *Biochemistry* **1999**, *38*, 16740−16748.
(32) Jorns, M. S.; Sancar, G. B.; Sancar, A. *Biochemistry* **1984**, *23*, 2673−2679.

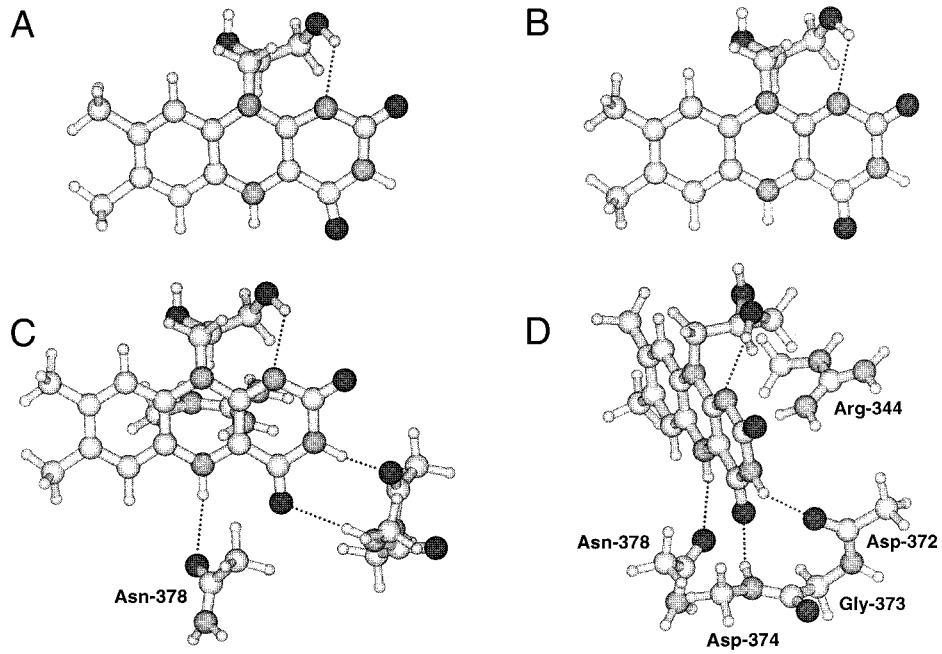

Figure 2. Truncated molecular models used for calculation purposes (see text for details): model 1 (A); model 2 (B); and model 3 (C, D).

distribution of the flavin radical, a guanidino cation residue placed at the Arg-344 position has also been included in our calculations. For computational purposes, all amino acids have been truncated, as indicated in the models shown in Figure 2. The geometries of the complexes were optimized at the semiempirical PM3 level. The calculations of spin densities and isotropic and anisotropic hfc's[33−35] were performed at the unrestricted Kohn−Sham level utilizing the Becke3 exchange functional combined with the Lee−Yang−Parr correlation functional, B3LYP,[36] as implemented in Gaussian 98.[37] Several basis sets, such as 6-31G*, 6-31G**, and the double-ζ basis set EPR-II,[33] have been used. The trends described below were observed with all these basis sets. For brevity, however, we will limit our discussion to results obtained using the EPR-II basis set which gave the best agreement with experimentally determined hfc's. The graphical representations of SOMOs and iso-spin density surfaces were achieved using the Molden program package.[38]

3. Results and Discussion

3.1. Model Geometries. The models used in our calculations are shown in Figure 2. Model 1 consists of the truncated flavin derivative (see Figure 1) where the heavy-atom positions have been obtained from the X-ray structure of *E. coli* DNA photolyase.[14] Protons have been added, and their respective positions were energy optimized while all heavy-atom positions were kept unchanged. After energy minimization, the proton at O3′ is found at a distance of 2.31 Å from N1 in the 7,8-dimethyl isoalloxazine ring and, hence, forms a weak intramolecular hydrogen bond.[14]

Model 2 consists of the same $FADH^{\bullet}$ fragment as that used in model 1; however, here both proton and heavy-atom positions in the 7,8-dimethyl isoalloxazine moiety have been energy optimized. The structure of the flavin semiquinone radical of model 1 was used as a starting point for the optimization. The heavy-atom coordinates of the ribityl side chain were kept unchanged since this hydroxy alkyl chain is held tightly in place by a hydrogen bond network to the protein environment. As a result of the energy minimization, the length of the intramolecular O3′−H···N1 hydrogen bond is increased slightly to 2.38 Å. With the C4a, N5, and N10 atom positions as reference (these are also the atoms bearing the highest electron spin density; see below), the displacements of atom positions of the refined structure of model 2 with respect to atom positions in model 1 are typically less than 0.4 Å. The differences in bond lengths between the heavy atoms of the two models are on average ±0.04 Å, which is well below the spatial resolution of 2.3 Å of the X-ray structure.[14] The most prominent adjustments in the refined model 2 structure are the shortened C8−C8α and C7−C7α bonds (1.49 and 1.48 Å, respectively, compared to 1.53 and 1.60 Å in model 1) and a more "relaxed" arrangement of the outer pyrimidine ring of the 7,8-dimethyl isoalloxazine moiety: in the model 2 structure, the angle N3−C4−O4 is increased to 118.3° (compared to 111.8° in model 1), while the angle O4−C4−C4a is reduced to 124.9° (compared to 132.1° in model 1).

The model 2 geometry shows significant deviations from the proposed vacuum structures of Zheng and Ornstein[17] and Meyer and co-workers,[16] with the most noticeable differences in the pyrimidine and pyrazine rings. In particular, longer N1−C2 (1.43 Å), N3−C4 (1.41 Å), and N10−C10a (1.43 Å) bonds are obtained in our model 2 structure, compared to 1.37, 1.37, and 1.36 Å of compound **5** in ref 17, whereas the N10−C1′ bond is shortened in model 2 (1.39 Å) compared to 1.46 Å.[17] In particular, an elongation of the C9a−N10 and N10−C10a bonds was obtained compared to previous studies. It should be noted

(33) Barone, V. In *Recent Advances in Density-Functional Methods, Part I*; Chong, D. P., Ed.; World Scientific Publishing: Singapore, 1995.
(34) Rega, N.; Cossi, M.; Barone, V. *J. Chem. Phys.* **1996**, *105*, 11060−11067.
(35) Barone, V. *Chem. Phys. Lett.* **1996**, *262*, 201−206.
(36) Becke, A. D. *J. Chem. Phys.* **1993**, *98*, 5648−5652.
(37) Frisch, M. J.; Trucks, G. W.; Schlegel, H. B.; Scuseria, G. E.; Robb, M. A.; Cheeseman, J. R.; Zakrzewski, V. G.; Montgomery, J. A.; Stratmann, R. E.; Burant, J. C.; Dapprich, S.; Millam, J. M.; Daniels, A. D.; Kudin, K. N.; Strain, M. C.; Farkas, O.; Tomasi, J.; Barone, V.; Cossi, M.; Cammi, R.; Mennucci, B.; Pomelli, C.; Adamo, C.; Clifford, S.; Ochterski, J.; Petersson, G. A.; Ayala, P. Y.; Cui, Q.; Morokuma, K.; Malick, D. K.; Rabuck, A. D.; Raghavachari, K.; Foresman, J. B.; Cioslowski, J.; Ortiz, J. V.; Stefanov, B. B.; Liu, G.; Liashenko, A.; Piskorz, P.; Komaromi, I.; Gomperts, R.; Martin, R. L.; Fox, D. J.; Keith, T.; Al-Laham, M. A.; Peng, C. Y.; Nanayakkara, C.; Gonzalez, M.; Challacombe, M.; Gill, P. M. W.; Johnson, B. G.; Chen, W.; Wong, M. W.; Andres, J. L.; Head-Gordon, M.; Replogle, E. S.; Pople, J. A. *Gaussian 98 (Revision A.7)*; Gaussian, Inc.: Pittsburgh, PA, 1998.
(38) Schaftenaar, G.; Noordik, J. H. *J. Comput.-Aided Mol. Design* **2000**, *14*, 123−134.

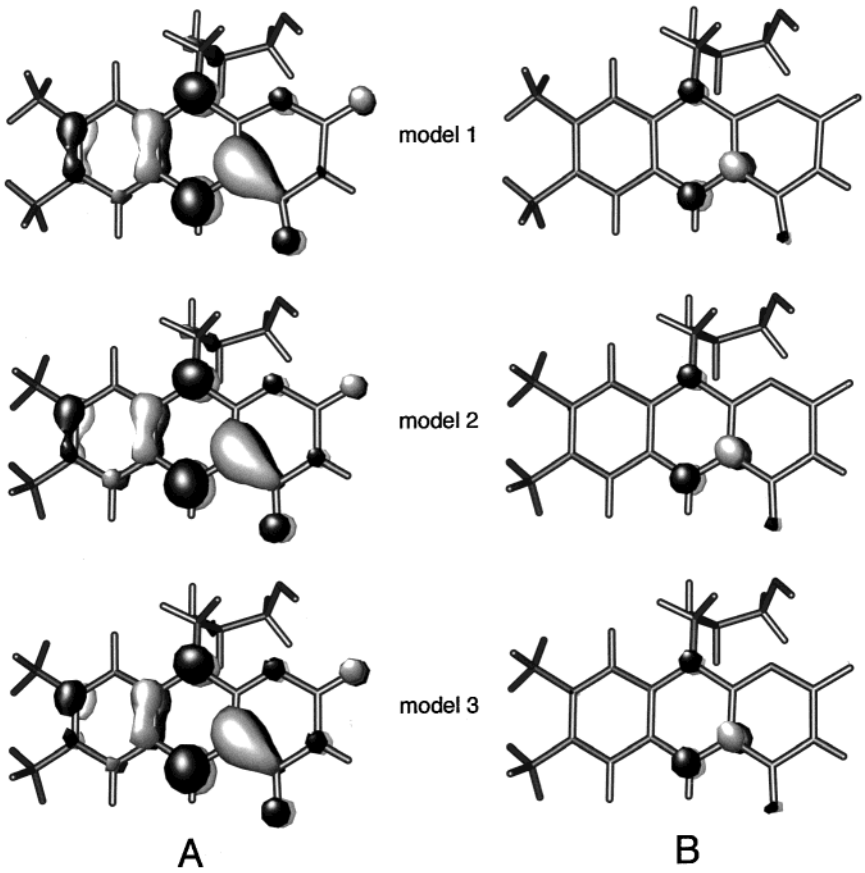

Figure 3. Singly occupied molecular orbitals (SOMOs) (0.05 (A) and 0.1 e/au^3 (B)) of the three models of Figure 2. The dark and light areas denote regions of opposite sign of the wave function. The protein environment of model 3 is not drawn, for clarity.

that the 7,8-dimethyl isoalloxazine ring system of our proposed structure is essentially planar, with a deviation from planarity of only 2.4° by folding along the N5−N10 axis. This very small ring puckering agrees well with Zheng and Ornstein's compound **5** structure;[17] however, a larger value of 8.0° was reported by Meyer and co-workers.[16] Ultimately, the validity of our proposed structures will be justified by comparison of the calculated hfc's with experimental determinations from EPR and ENDOR experiments[31] that provide a direct measure of the geometry-dependent spin densities at the respective nuclei (see below).

The model 3 geometry is based on the structure of model 2. Additionally, truncated amino acid fragments have been placed at the positions of Arg-344, Asp-372, Gly-373, Asp-374, and Asn-378 to mimic the protein environment of the FAD cofactor in *E. coli* DNA photolyase (Figure 2). Hydrogen bond lengths of 2.00 Å for N3−H···O of Asp-372, 2.36 Å for N5−H···O of Asn-378, and 2.56 Å for O4···H−N of Asn-374 were obtained. The Cartesian coordinates of all three models used in our calculations may be obtained upon request from the corresponding author and are listed in the Supporting Information.

3.2. Spin Densities. The singly occupied molecular orbitals (SOMO ≡ α-HOMO) of all three models are compared in Figure 3 at two electron density contour values, (A) 0.05 and (B) 0.1 e/au^3. The tighter contours in Figure 3B show that the electron density of the SOMO of FADH• is concentrated at the O4, C4a, N5, and N10 atom positions, with the highest concentration found at C4a and N5. The diffuse contour at 0.05 e/au^3 encompasses the majority of the electron density within the SOMO. Significant electron density is additionally found at N1, O2, C5a, C8, and C9a. The SOMO plots of all three models are very similar for most parts of the FADH• radical, but there are discernible differences at the N3 and C7 atom positions. Compared to model 1, the electron density at N3 in model 2 is increased, as a result of the rearrangement of the pyrimidine ring in the 7,8-dimethyl isoalloxazine moiety upon geometry optimization. A further increase is observed due to hydrogen bonding of the proton at N3 to the carbonyl oxygen in the nearby amino acid Asp-372 (model 3). Introduction of the pseudo-protein environment also has a discernible effect on the electron density distribution in the outer benzene ring: a noticeable enrichment of electron density is observed at C8, while the positions C6 and C7 are impoverished (see below). EPR and ENDOR methods, via the hfc's, measure the interaction of the magnetic nuclei with the unpaired spin in the radical. To a first approximation, the unpaired spin density should correspond to the electron density within the SOMO. However, due to exchange interactions between the SOMO electron and other electrons with equal M_S electron spin components in different but symmetry-equivalent orbitals, regions of net negative electron-spin density (excess β) and net positive electron-spin density (excess α) within the radical arise. In π-type organic radicals, this $\sigma-\pi$ correlation is often called spin polarization.[39−41] As can be seen from Figure 4, the electron density distributions of the SOMO are mirrored in the positive ($\alpha - \beta$) unpaired spin density contours: the highest concentrations of net positive spin density are found at O4, C4a, N5, and N10. Spin polarization leads to significant net negative spin density at the C2, C5a, C9, and C10a positions.

The anisotropic and isotropic hfc's calculated for the heavy-atom nuclei in the isoalloxazine moiety are presented in Table 1. Finite spin density at the nucleus of an atom arises if an orbital

(39) McConnell, H. M. *J. Chem. Phys.* **1956**, *24*, 764−766.
(40) Bersohn, R. *J. Chem. Phys.* **1956**, *24*, 1066−1070.
(41) Weissman, S. I. *J. Chem. Phys.* **1956**, *25*, 890−891.

Table 1. Isotropic (A_{iso}) and Anisotropic (T) Hyperfine Couplings Calculated for the Heavy Atoms in the 7,8-Dimethyl Isoalloxazine Moiety of FADH• (All Values Given in MHz)

atom	model 1		model 2		model 3	
	T_{11} T_{22} T_{33}	A_{iso}	T_{11} T_{22} T_{33}	A_{iso}	T_{11} T_{22} T_{33}	A_{iso}
C2	2.7		1.8		1.8	
	0.7	−11.1	0.2	−7.1	0.2	−4.8
	−3.4		−2.0		−2.0	
C4	1.3		1.5		3.3	
	0.7	−18.3	0.5	−19.2	−0.5	−13.7
	−2.0		−2.0		−2.8	
C4a	59.2		57.7		53.0	
	−29.2	27.8	−28.5	21.1	−26.0	16.4
	−30.0		−29.2		−27.0	
C5a	2.9		3.2		2.7	
	0.5	−11.8	0.9	−13.7	0.5	−14.4
	−3.4		−4.1		−3.2	
C6	6.9		8.6		8.2	
	−3.1	3.9	−4.0	4.9	−3.8	4.4
	−3.8		−4.6		−4.4	
C7	0.7		0.9		0.9	
	0.4	−4.6	0.7	−5.0	0.7	−4.8
	−1.1		−1.6		−1.6	
C8	11.0		12.8		14.1	
	−5.2	6.2	−6.1	6.7	−6.7	8.0
	−5.8		−6.7		−7.4	
C9	2.2		2.6		3.2	
	1.4	−5.2	1.7	−6.2	2.2	−7.3
	−3.6		−4.3		−5.4	
C9a	9.5		10.0		11.5	
	−4.6	3.0	−4.8	3.0	−5.6	2.9
	−4.9		−5.2		−5.9	
C10a	4.9		3.1		2.9	
	2.3	−28.0	0.9	−21.2	0.8	−19.1
	−7.2		−4.0		−3.7	
C7α	0.3		0.3		0.3	
	−0.1	0.2	−0.1	0.3	−0.1	0.1
	−0.2		−0.2		−0.2	
C8α	0.2		0.3		0.2	
	0.0	−2.5	0.0	−3.1	0.1	−3.5
	−0.2		−0.3		−0.3	
C1′	1.2		1.2		1.1	
	0.0	−3.9	0.0	−3.9	0.0	−4.9
	−1.2		−1.2		−1.1	
N1	8.5		4.9		3.1	
	−4.1	6.7	−2.4	3.5	−1.5	1.1
	−4.4		−2.5		−1.6	
N3	0.3		0.4		1.5	
	0.0	−1.8	0.0	−1.7	−0.6	−0.3
	−0.3		−0.4		−0.9	
N5	27.4		27.7		29.6	
	−13.6	13.2	−13.8	11.0	−14.7	13.1
	−13.8		−13.9		−14.9	
N10	13.4		13.3		14.8	
	−6.6	5.9	−6.5	5.9	−7.3	8.3
	−6.8		−6.8		−7.5	
O2	10.0		6.8		6.6	
	9.8	−5.7	6.7	−4.0	6.4	−2.9
	−19.8		−13.5		−13.0	
O4	11.9		14.8		11.5	
	11.3	−6.2	14.6	−8.7	11.1	−5.3
	−23.2		−29.4		−22.6	

of spherical symmetry contributes to the MO occupied by the unpaired electron spin. Such s-orbital spin density leads to isotropic hfc's; the contribution is called Fermi contact interaction.[42,43] It has been observed that experimental ^{13}C hyperfine splittings are not simply proportional to the π-spin population on the respective carbon atom. Rather it is also necessary to include contributions from the π-spin density on neighboring atom positions. For the isotropic hfc's of ^{13}C atoms within the molecular framework of the π-system, π-spin density at the atom itself contributes positively, whereas π-spin density on near-neighboring atoms contributes negatively. Hence, the C4a position with high electron density (see Figure 3) has a large positive isotropic hfc. Smaller positive values are observed for the atoms C6, C8, and C9a. Large negative isotropic hfc's were calculated for the atoms C4, C5a, C9, and C10a, reflecting spin polarization from the large π-spin density on the adjacent positions O4, N5, C6, C8, C9a, and N10. Similarly, positive ^{14}N isotropic hfc's are found for the nitrogens N5 and N10. Large π-spin density at ^{17}O atoms itself contributes negatively as a result of the negative magnetic moment of ^{17}O. Consequently, negative values are observed for O4 and O2.

Anisotropic contributions to the hfc's arise from spin density of the unpaired electron spin in orbitals with nonspherical symmetry and vanishing electron density at the nucleus. The spin density plots of Figure 4 are a direct reflection of this orientation-dependent contribution to the hfc's. Axially symmetric hyperfine tensors with large anisotropy are observed for the nuclei O2, O4, C4a, N5, C6, C8, C9, C9a, and N10, which carry high spin density. Rhombic tensors with smaller anisotropy are found at C4, C5a, and C10a. Relatively small magnitude principal hyperfine tensor values are found for the other atom positions which have small positive or negative spin density.

Calculated isotropic and anisotropic hfc's of protons are listed in Table 2. Typically, isotropic hfc's of α-protons within a π-system arise from spin polarization and reflect the unpaired spin density on the neighboring carbon or nitrogen atoms. Hence, for the protons H5 and H6, which are bound to nitrogen and carbon with high spin densities, negative isotropic hfc's are observed, due to spin polarization from N5 and C6, respectively. Similarly, the negative π-spin density at C9 is reflected by the positive hfc of H9. With the exception of H5, the hyperfine tensors of the α-protons are nearly axial symmetric.

The distances of β-protons to the π-spin system are rather large, and their dipolar couplings are, therefore, relatively small. They may have a large contact hyperfine interaction, however, caused by hyperconjugation.[44,45] Further discussion of the proton hfc's will be given below.

3.3. Protein Binding of FADH•. As described in the Computational Methods section, we have modeled hydrogen-bonding interactions by inclusion of truncated amino acid fragments with their heavy-atom positions taken from the X-ray structure.[14] The geometries of model 2 and model 3 differ only in the absence and presence of the surrounding protein environment, respectively. All atom positions within the flavin cofactor are identical. This allows us to directly assess the influence of protein binding on the electron density and unpaired spin density distribution. Comparing the spin density plots of model 2 and model 3 reflecting the anisotropic hfc's (Figure 3), the most noticeable differences are observed at the atom positions N1 and O4, where the amplitude of the axially symmetric hyperfine tensors are decreased, and at the atom positions N3 and C4 with an increasing spin density in orbitals with nonspherical symmetry. Smaller changes are observed at C4a, C5a, C8, C9, C9a, N5, and N10. It is noteworthy that the electron density is affected not only at positions with direct hydrogen bonding to the protein

(42) Atherton, N. M. *Principles of Electron Spin Resonance*; Ellis Horwood Ltd.: Chichester, 1993.

(43) Weil, J. A.; Bolton, J. R.; Wertz, J. E. *Electron Paramagnetic Resonance*; John Wiley & Sons: New York, 1994.

(44) Bolton, J. R.; Carrington, A.; McLachlan, A. D. *Mol. Phys.* **1962**, *5*, 31−41.

(45) Colpa, J. P.; de Boer, E. *Mol. Phys.* **1963**, *7*, 333−348.

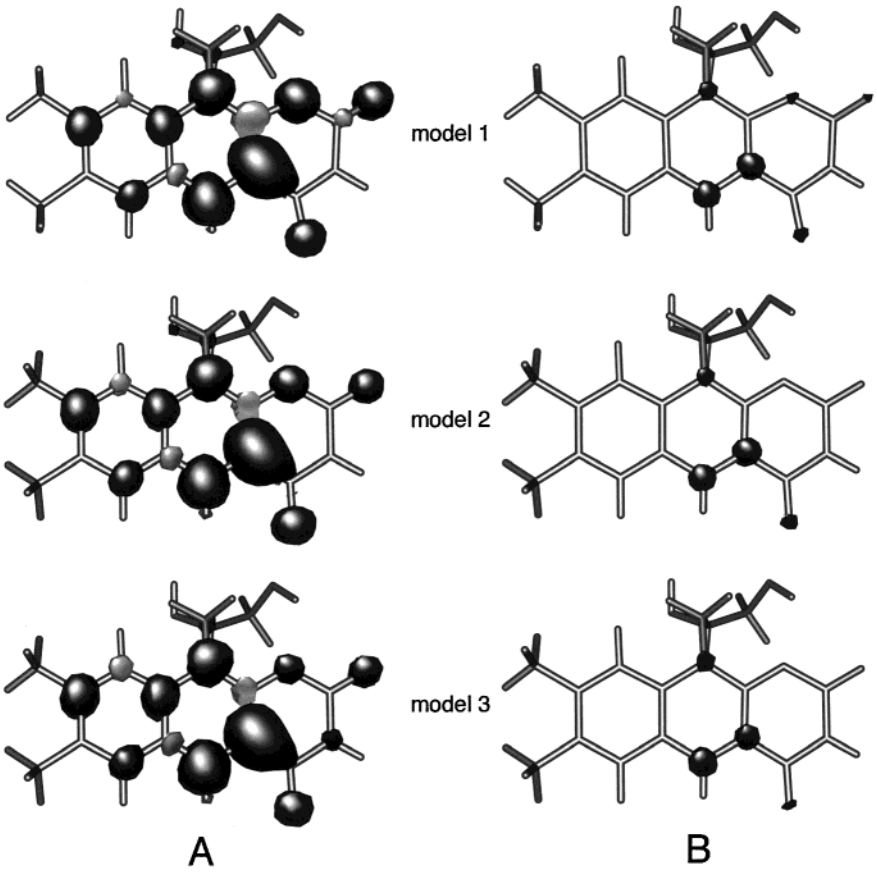

Figure 4. Unpaired iso-spin density surfaces (0.002 (A) and 0.02 e/au^3 (B)) for the three radicals of Figure 2. Dark gray and light gray color of surfaces indicates positive and negative spin density, respectively. The protein environment of model 3 is not drawn, for clarity.

environment but also at atoms remote from hydrogen bonds. It is difficult to visualize the subtle shifts of the total unpaired electron spin density when comparing the iso-spin density spheres of the models 2 and 3 (Figure 4). Therefore, we prefer to depict differences in spin densities at the positions of the nuclei that lead to changes of isotropic hfc's upon inclusion of the pseudo-protein environment. These changes are depicted in Figure 5. Increasing absolute spin density at the nucleus is depicted by drawn line symbols, whereas a decrease of spin density is shown by dotted line symbols. Clearly, no significant spread of spin density is observed over the cofactor environment, with the one exception of the NH1 in the guanidino residue of Arg-344, where a small positive isotropic spin density is found. This spin density shift can be understood in terms of a direct interaction of the positively charged guanidino residue with the π-spin system of the 7,8-dimethyl isoalloxazine moiety brought about by its close proximity perpendicular to the π-plane. The majority of the unpaired electron spin remains confined on the 7,8-dimethyl isoalloxazine moiety, but a significant redistribution of spin density occurs (Figure 5). Isotropic spin density arising from spin polarization is reduced on the outer pyrimidine ring and shifted to the central pyrazine ring and, to a lesser extent, to the outer benzene ring, with the most noticeable changes of increasing positive hfc's at N5 and N10. Changes in spin density are unequally distributed in the benzene ring. While in the lower half of the benzene ring spin density is reduced, e.g., at C6 and C7, an increase in spin density is observed in the upper half at C8 and C9. A similar increase is observed at positions C1′ and C2′ in the ribityl side chain.

The redistribution of spin density in the 7,8-dimethyl isoalloxazine has stimulated us to examine FADH• models where only single amino acid residues are present, i.e., either Arg-344, Asp-372, Gly-373, Asp-374, or Asp-378 (results not shown). Surprisingly, no uniform trend like the one described above is observed when single amino acids are hydrogen-bonded to the FAD cofactor. Rather, nonuniform changes are observed. Therefore, we conclude that the above-mentioned spin redistribution is a result of a concerted action of the protein environment and, thus, is important for fine-tuning the electronic structure of the FAD cofactor in order to optimize its specific enzymatic function. Protein−cofactor interactions, which modulate the electron density in order to influence the redox potential of the flavin, have been discussed recently.[46,47]

3.4. Comparison with Experimental Determinations of Proton Hyperfine Couplings. Proton ENDOR/TRIPLE experiments have been performed on the neutral flavin radical cofactor of DNA photolyase from *E. coli*.[31] A comparison between calculated and experimental hfc's is presented in Table 3.

The largest proton hfc arises from the proton at N5. Although only one component of the rhombic hyperfine tensor could be resolved from ENDOR,[31] an isotropic value of −23 MHz has been reported, based on the characteristic splitting of continuous-wave EPR spectra. This experimental value for A_{iso} compares very favorably with our calculated value of −24.1 MHz, obtained from our most elaborate computation based on the geometry-optimized FADH• including the pseudo-protein environment, model 3. Certainly, the H5 is very close to positions bearing the highest spin density on the 7,8-dimethyl isoalloxazine moiety, and hence, it would be most desirable to have a full characterization of all hfc tensor components. Clearly,

(46) Breinlinger, E.; Niemz, A.; Rotello, V. M. *J. Am. Chem. Soc.* **1995**, *117*, 5379−5380.
(47) Ghisla, S.; Massey, V. *Eur. J. Biochem.* **1989**, *181*, 1−17.

Table 2. Isotropic (A_{iso}) and Anisotropic (T) Hyperfine Couplings Calculated for the Protons in the 7,8-Dimethyl Isoalloxazine Moiety of FADH• (All Values Given in MHz)

atom	model 1		model 2		model 3	
	T_{11}		T_{11}		T_{11}	
	T_{22}	A_{iso}	T_{22}	A_{iso}	T_{22}	A_{iso}
	T_{33}		T_{33}		T_{33}	
H3	1.6		2.0		2.7	
	−0.2	−0.5	−0.6	−0.7	−1.2	−1.9
	−1.4		−1.4		−1.5	
H5	21.9		22.0		23.5	
	−4.6	−18.6	−4.7	−21.6	−4.9	−24.1
	−17.3		−17.3		−18.6	
H6	2.8		2.9		3.0	
	−1.1	−3.8	−1.2	−4.4	−1.2	−4.4
	−1.7		−1.7		−1.8	
H9	2.0		2.0		2.3	
	−0.7	1.0	−0.6	1.4	−0.8	1.7
	−1.3		−1.4		−1.5	
H1′l	2.4		2.4		2.6	
	−1.1	0.7	−1.1	0.9	−1.3	1.1
	−1.3		−1.3		−1.3	
H1′r	2.5		2.6		2.8	
	−0.7	11.6	−0.9	10.9	−1.1	12.1
	−1.8		−1.7		−1.7	
	A_{11}		A_{11}		A_{11}	
	A_{22}	A_{iso}	A_{22}	A_{iso}	A_{22}	A_{iso}
	A_{33}		A_{33}		A_{33}	
$CH_3(7\alpha)$[a]	0.5		0.1		0.2	
	−0.6	−0.3	−1.1	−0.8	−1.0	−0.7
	−0.8		−1.3		−1.2	
$CH_3(8\alpha)$[a]	6.0		8.1		9.2	
	4.6	5.0	6.5	7.0	7.5	8.0
	4.4		6.3		7.3	

[a] For the methyl group protons, the total (isotropic plus anisotropic) principal values (A) are given. These are obtained by averaging over the values calculated for a static orientation of the three hydrogens.

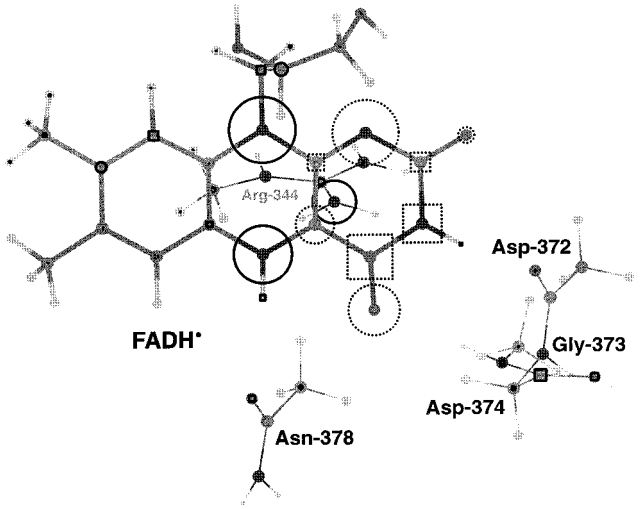

Figure 5. Changes in s-spin density upon protein binding of FADH• to Arg-344, Asp-372, Gly-373, Asp-374, and Asn-378. Circles and squares represent positive and negative s-spin density, respectively. Increasing absolute spin density at the nuclei is depicted by full line symbols, whereas a decrease of spin density is shown by dotted line symbols.

additional experiments are necessary to resolve this very broad feature that remains unresolved in continuous-wave ENDOR.

The second largest hfc arises from one of the (magnetically inequivalent) protons attached to C1′. The distance of these protons to N10 bearing high spin density is rather large, and the anisotropic dipolar coupling is, therefore, relatively small.

Table 3. Comparison of Experimental[31] and Calculated Isotropic Proton Hyperfine Couplings in the 7,8-Dimethyl Isoalloxazine Moiety of FADH• of *E. coli* DNA Photolyase (All Values Given in MHz)

	model 1	model 2	model 3	expt
H5	−18.6	−21.6	−24.1	−23
H1′l	0.7	0.9	1.1	2.7
H1′r	11.6	10.9	12.1	9.0
H6	−3.8	−4.4	−4.4	−4.86
$CH_3(8\alpha)$	5.0	7.0	8.0	7.49

The isotropic hfc may still be large but, importantly, varies with the twist angle between the N10's $2p_z$ orbital and the C1′−H bond. Using a hyperconjugation model, a $\cos^2\theta$ dependence of the splitting is expected,[48,49] where θ is the dihedral angle between the $2p_z$ orbital of N10 and the C1′−C2′ bond. Usually, the result is that one of the two β-protons is coupled more strongly than the other. The ratio of these hfc's, therefore, reflects the geometrical arrangement of the ribityl side chain with respect to the π-plane of FADH•. We predict axial symmetry for the hfc tensors of both protons at C1′, which is also in agreement with the experiment. However, our calculated values for A_{iso} for H1′l and H1′r of 1.1 and 12.1 MHz, respectively, do not fit so well with the experimental values of 2.7 and 9.0 MHz, respectively. But, given the $\cos^2\theta$ dependence of these couplings, a small rotation of the ribityl side chain can have a large effect on these couplings. As was noted in ref 31, the ratio of the experimental hfc's from these two protons rather reflects the cofactor geometry determined for the *Anacystis nidulans* DNA photolyase[50] than that of the enzyme isolated from *E. coli*.[14] This is perhaps not surprising as the *A. nidulans* photolyase structure was determined at higher resolution and, the cofactor binding site of both structures is conserved. In the present calculations we have, nevertheless, used the *E. coli* DNA photolyase structure for consistency and have conserved the geometry of the ribityl side chain with respect to the 7,8-dimethyl isoalloxazine moiety. Thus, taking the side-chain geometry of the higher resolution structure brings the calculated values into very good agreement with the experimental ones (results not shown).

A slightly smaller hfc with much weaker intensity, which is also often observed in the ENDOR spectra of flavin radicals, is that arising from the proton at C6. This is an α-proton, and its hfc tensor would be expected to be of rhombic shape, as is confirmed by our calculations. Very often, however, only the central crossing point in the powder ENDOR spectrum of this tensor is visible.[31,51−53] It is usually assigned to A_{iso}, which is a good assumption as long as the tensorial pattern is symmetric around A_{iso} (i.e., $T_{11} = -T_{33}$). This is not quite the observed case, so further experiments to fully characterize this hfc are necessary. Nevertheless, the observed transition at −4.86 MHz for the proton at C6 in DNA photolyase is still in good agreement with our calculated value of −4.4 MHz.

Perhaps the most characteristic and easy-to-distinguish feature in the proton ENDOR spectra of flavoenzymes is the coupling

(48) Heller, C.; McConnell, H. M. *J. Chem. Phys.* **1960**, *32*, 1535−1539.
(49) Horsfield, A.; Morton, J. R.; Whiffen, D. H. *Mol. Phys.* **1961**, *4*, 425−431.
(50) Tamada, T.; Kitadokoro, K.; Higuchi, Y.; Inaka, K.; Yasui, A.; de Ruiter, P. E.; Eker, A. P. M.; Miki, K. *Nature Struct. Biol.* **1997**, *4*, 887−891.
(51) Medina, M.; Gómez-Moreno, C.; Cammack, R. *Eur. J. Biochem.* **1995**, *227*, 529−536.
(52) Macheroux, P.; Petersen, J.; Bornemann, S.; Lowe, D. L.; Thorneley, R. N. F. *Biochemistry* **1996**, *35*, 1643−1652.
(53) Çinkaya, I.; Buckel, W.; Medina, M.; Gómez-Moreno, C.; Cammack, R. *Biol. Chem.* **1997**, *378*, 843−849.

Table 4. Comparison of Experimental Isotropic Hyperfine Couplings for the $CH_3(8\alpha)$ and H6 Protons in Neutral Flavin Radical Enzyme Cofactors (All Values Given in MHz)[a]

protein	$CH_3(8\alpha)$	H6	ref
DNA photolyase from *E. coli*	7.49	−4.86	31
flavodoxin from *Azotobacter vinelandii*	8.3	(−)5.5	54
flavodoxin from *Megasphaera elsdenii*	8.5	(−)5.6	54
ferredoxin-$NADP^+$ reductase	8.12	(−)5.11	51
chorismate synthase	8.58	(−)6.3	52
4-hydroxybutyryl-CoA dehydratase	8.5	(−)6.23	53

[a] Signs in parentheses have not been determined experimentally.

belonging to the methyl protons at C8α. They have, therefore, often been used in experimental studies as a sensitive indicator of the spin density distribution on the benzene ring of the 7,8-dimethyl isoalloxazine moiety in flavins.[51−53] The hfc tensor of the protons at C8α has axial symmetry and a small anisotropy typical for a freely rotating methyl group. The experimental A_{iso} = 7.49 MHz is the smallest hfc for an enzyme with a neutral flavin radical cofactor reported so far[31] (see Table 4).

From the X-ray structures of DNA photolyase,[14,50] it is known that the FAD is mostly buried in the protein and not exposed to the aqueous phase, which is not the case for most other flavoproteins. In frozen solution, nearby water molecules which interact with the π-system could be responsible for increasing the hfc's in the other flavoproteins with respect to those in DNA photolyase. An analogous effect has been observed for nitroxides and quinones: in nonpolar environments the hfc's were reduced with respect to those measured in polar and/or protic solvents.[55−57] Aqueous and relatively nonpolar environments have very different dielectric constants, which strongly affect electron-transfer rates, due to their effect on the reorganization energy. In model photolyase systems, Heelis and co-workers showed that the quantum yield of splitting *cis,syn*-1,3-dimethyluracil dimers is solvent dependent, due to changes in the relative rates for forward and backward electron transfer.[3] With a small reorganization energy, due to the nonpolar environment, the back transfer is highly exogenic and, hence, probably in the Marcus inverted region. It may be, therefore, that DNA photolyase uses a low-polarity site for the $FADH^-$ in order to slow the back electron transfer, k_{-1}, and thereby to increase the yield of dimer splitting (eq 2). $FADH^•$ is the intermediate electron acceptor in the DNA repair process in living cells, and its local dielectric environment is reflected in its hfc's.

In concluding this comparison, it is fair to state that the proton hfc's of the $FADH^•$ cofactor from DNA photolyase could be reliably predicted using the hybrid B3LYP functional in conjunction with the EPR-II basis set. It is unfortunate that so far no ^{13}C, ^{15}N, and ^{17}O hfc's have been reported for this species. However, the good agreement between experimental and calculated proton hfc's suggests that the wave function is well described and the predicted values for the heavy atoms provide a solid basis for the experimental determination and assignment of hfc's in future flavin studies.

3.5. Relevance for Enzyme Function. At least two types of photoreactions have been observed experimentally in DNA photolyase: (a) photorepair of damaged DNA by the catalytically active enzyme with its flavin cofactor initially in the fully reduced state,[9,10] $FADH^-$ (eqs 1−3), and (b) photoreduction of the catalytically inert enzyme[19−21] when the flavin cofactor is in a redox state different from $FADH^-$, i.e., $FADH^•$ or FAD_{ox}. In both electron-transfer processes, the flavin in its radical (semiquinone) form, $FADH^•$, is involved as an electron acceptor and/or as an important intermediate in the enzymatic pathway. In this contribution we will restrict our discussion to the DNA repair process.

DNA photorepair by photolyases starts out from the excited singlet state of $FADH^-$ and proceeds via electron donation from the flavin cofactor to the DNA lesion where the excess electron is utilized to initiate a [2 + 2] cycloreversion of the T⟨⟩T dimer. The repair efficiency of the enzyme is optimized by minimizing the rate of back electron transfer, k_{-1}, with respect to the rate of forward electron transfer, k_1 (eq 1). This may be achieved by transferring the electron over a wide distance, possibly through one or more intermediate electron acceptors, as is, for example, accomplished in the primary charge separation of bacterial and plant photosynthesis. Once the cyclobutane ring of T⟨⟩T is split, electron transfer from the repaired, i.e., cleaved, TT segment back to $FADH^•$ (see eq 3) has to occur rapidly in order to deactivate the highly reactive radical anion species $TT^{•-}$. Here, too large a cofactor−substrate distance is detrimental for repair efficiency, since the rate of electron transfer decreases exponentially with increasing distance between $TT^{•-}$ and $FADH^•$. Without the X-ray structure of a cocrystal of a photolyase with a bound DNA substrate being available, estimates of the distance between the T⟨⟩T lesion and $FADH^•$ rely on modeling.[58−61]

In two of the three molecular dynamics studies, the minimum distance between the flavin cofactor and the base pair containing the *cis,syn*-cyclobutane thymine dimer was at least 6 Å when model dinucleotides and related derivatives were examined.[59,60] Substantially wider distances are predicted when single-strand or duplex oligonucleotides containing a T⟨⟩T lesion are studied.[59] In these more realistic systems, the nonpolar cyclobutane moiety of the dimer is at least 10 Å away from the 7,8-dimethyl isoalloxazine moiety of $FADH^•$. On the other hand, in the third molecular dynamics study, a very short distance of less than 3 Å for the substrate−cofactor distance was suggested.[61] This latter model is supported by experimental work of Vande Berg and Sancar,[58] who have predicted a van der Waals contact between T⟨⟩T and FAD on the basis of measured quantum yields and substrate association constants that were determined for various point mutations of yeast DNA photolyase from *Saccharomyces cerevisiae*.

To date, this dispute has not been settled. However, it is clear that in DNA repair $FADH^•$ selectively obtains an electron from the cleaved T⟨⟩T fragment with the electron-transfer pathway, direct or via superexchange, still not clarified. Two factors in the spatial and electronic structure of the FAD in DNA photolyases point to the superexchange-mediated pathway. First, the FAD has a unique and characteristic U-shaped configuration[14,50,62] in which the adenine ring is bent over the 7,8-dimethyl isoalloxazine moiety, bringing it into close proximity to N5,

(54) Kurreck, H.; Bock, M.; Bretz, N.; Elsner, M.; Kraus, H.; Lubitz, W.; Müller, F.; Geissler, J.; Kroneck, P. M. H. *J. Am. Chem. Soc.* **1984**, *106*, 737−746.
(55) Kawamura, T.; Matsunami, S.; Yonezawa, T. *Bull. Chem. Soc. Jpn.* **1967**, *40*, 1111−1115.
(56) Joela, H.; Lehtovuori, P. *Phys. Chem. Chem. Phys.* **1999**, *1*, 4003−4010.
(57) Steinhoff, H.-J.; Savitsky, A.; Wegener, C.; Pfeiffer, M.; Plato, M.; Möbius, K. *Biochim. Biophys. Acta* **2000**, *1457*, 253−262.
(58) Vande Berg, B. J.; Sancar, G. B. *J. Biol. Chem.* **1998**, *273*, 20276−20284.
(59) Sanders, D. B.; Wiest, O. *J. Am. Chem. Soc.* **1999**, *121*, 5127−5134.
(60) Hahn, J.; Michel-Beyerle, M.-E.; Rösch, N. *J. Phys. Chem. B* **1999**, *103*, 2001−2007.
(61) Antony, J.; Medvedev, M.; Stuchebrukhov, A. A. *J. Am. Chem. Soc.* **2000**, *122*, 1057−1065.
(62) Hahn, J.; Michel-Beyerle, M. E.; Rösch, N. *J. Mol. Model.* **1998**, *4*, 73−82.

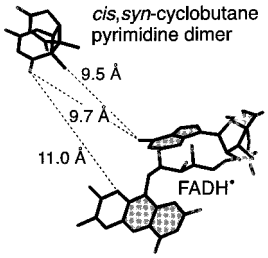

Figure 6. Putative relative position of the *cis*,*syn*-cyclobutane pyrimidine dimer with respect to the FAD cofactor in *E. coli* DNA photolyase, based on model calculations.[59] For this figure, the coordinates of a duplex DNA fragment bound to the DNA photolyase enzyme were used (for details, see ref 59). For clarity, only the heavy atoms of the truncated T⟨⟩T fragment in the DNA and the flavin cofactor are displayed.

N10, and C4a. Second, as borne out by our previous experiments, the electron density on the benzene ring of FADH• is very low. This is manifested by the smallest detected isotropic proton hfc of an 8-methyl group in a neutral flavin radical in flavoenzymes (see Table 4). Our present calculations fit well with these observations and further allow us to present a model of the SOMO on the 7,8-dimethyl isoalloxazine ring (see Figure 3). The SOMO has especially large amplitudes on the central pyrazine and the pyrimidine rings, thus increasing orbital overlap between the π-systems of the 7,8-dimethyl isoalloxazine and adenine moieties of FADH (see Figure 6).

Taken together, this suggests that electron transfer to and from the DNA lesion possibly proceeds via the adenine moiety. This enables a superexchange-type mechanism[63] in which intermediate electronic states of the adenine cause an effective coupling between the redox-active isoalloxazine and the T⟨⟩T lesion without the necessity of a direct orbital overlap between these redox partners.

(63) Bolton, J. R.; Mataga, N.; McLendon, G. *Electron Transfer in Inorganic, Organic, and Biological Systems*; American Chemical Society: Washington, DC, 1989.

4. Conclusions

In the present work, we have undertaken a detailed analysis of geometries, spin properties, and hyperfine structures of the neutral flavin radical in a vacuum and under the influence of the specific protein environment in the DNA photolyase enzyme. The hfc's calculated using density functional theory are in favorable agreement with experimental determinations from previous EPR, ENDOR, and TRIPLE studies. The best agreement is obtained when amino acid fragments are taken into account in order to mimic the natural cofactor environment of FADH• in DNA photolyase.

It is found that the specific protein environment of FAD in DNA photolyase causes a significant redistribution of both the electron and spin densities, thus fine-tuning the electron-transfer properties of the cofactor. Spin and electron densities are highest in the central pyrazine and outer pyrimidine rings of FADH•, thus maximizing orbital overlap with the π-system of the adjacent adenine ring. This facilitates a superexchange-mediated electron transfer to and from the CPD lesion in the DNA repair process. The relevance of our results to the photoreduction process will be discussed in a future contribution.

Acknowledgment. It is a pleasure to thank Professor A. Bacher (Technical University Munich) for his continuous support and encouragement. We thank Dr. Jens Törring (Free University Berlin, Germany) and Dr. Georg Gescheidt (University Basel, Switzerland) for valuable discussions. This work was supported by the Deutsche Forschungsgemeinschaft (SFB-498 and SFB-533), which is gratefully acknowledged.

Supporting Information Available: Cartesian coordinates of all structures discussed (PDF). This material is available free of charge via the Internet at http://pubs.acs.org.

JA003426M